Final Draft
of the original manuscript:

Pinheiro, G.; Olea, C.A.W.; dos Santos, J.F.; Kainer, K.U.:
Microstructural and Mechanical Behavior of Friction Welds in a High Creep Resistance Magnesium Alloy
In: Advanced Engineering Materials (2007) Wiley

DOI: 10.1002/adem.200700159

Microstructural and mechanical behavior of friction welds in a high creep resistance magnesium alloy**

By *Gustavo Alves Pinheiro, Cesar Afonso Weis Olea, Jorge Fernandez dos Santos and Karl Ulrich Kainer*[*]

The Mg alloys currently used in the automotive industry are high pressure die cast and have either high strength (AZ91D) or high ductility (AM60 and AM50) at room temperature. However, power train applications such as automatic transmission cases and engine blocks are limited for these alloys since their mechanical properties decrease rapidly with temperature. Mg-Si alloys, like AS21, AS41A and AS41B were exploited on a large scale in the various generation of the Volkswagen Beetle engine in the 70's. Nowadays magnesium engine blocks are rarely manufactured due to high operating temperature requirements of modern engines and the cost of the alloys.[1-3]

The die cast alloy AE42 has shown superior mechanical properties in applications at high temperatures. This alloy was developed from a non-aluminum magnesium chemistry in which rare earths, under die-casting conditions, were shown to increase creep resistance by forming fine Mg_9RE second phase particles along the grain boundaries. The presence of alloying elements results in significant advantages in comparison to Mg-Zn and Mg-Mn alloys. Rare earth elements presented in the commercially available AE alloys typically consists of Ce (>45%), La (20-30%), Nd (10-20%) and Pr (4-10%).[4-6] Table 1 shows a brief comparison between some materials industrially used.

Friction welding (FW) is a relatively unexplored area within Mg research and has shown some advantages as short welding times, good repeatability and suitability to perform sound welds especially in dissimilar configuration. Additionally, conventional fusion welding of lightweight materials generally produces a weld which suffers from defects such as liquation induced cracking or hot tearing and porosity, developed as a consequence of entrapped hydrogen gas not being able to escape from the weld pool during solidification. In the basic and most used variation one of the workpiece rotates while the other is held stationary. Both welding surfaces come in contact under a defined pressure during a preset time or upsetting. Owing to the frictional heating, plastic deformation takes place typically at temperatures below that of the absolute melting temperature of the alloy being joined. The material at the faying surfaces becomes plasticized and the parts are forged together at the end of the process. A schematic of the FW process is presented in Figure 1.

Table 1: Mechanical Properties of some industrial Mg- and Al-alloys.[7,8]

Mechanical Properties	AZ91D-F	AE42-F	AA2024-O	AA5083-O
Hardness (HB)	66	60	47	77
Rm (MPa)	230	234	186	290
$Rp_{0,2}$ (MPa)	150	145	75,8	145
Elongation (%)	6	11	20~22	22

Mg alloys features a number of characteristics, such as good heat conduction, high coefficient of linear thermal expansion and ease of oxidation, which affect the general weldability of these alloys. Nevertheless, new advances in joining technology have demonstrated their aptitude to be welded. Many publications describe the weldability of magnesium and its alloys through friction welding as possible.[9-13] Many research programs involving Mg similar and dissimilar joints with different alloys have been carried out aiming at an optimization of process parameters, leading to sound and reliable joint formation of friction welds.

Dissimilar magnesium friction welded joints have shown generally no significant loss of hardness across the bonding line with dynamic recrystallisation processes taking place along an app. 500µm wide stripe starting from the bonding line.[9] In similar welds macro and microstructures in the vicinity of the joint are symmetrical in relation to the weld interface and joint axis regardless of the applied friction time and of which one is the rotating workpiece. Tensile strength and elongation tend to improve with an increase in the friction pressure and friction time while the highest impact value observed was app. 60% of the base material due to the disappearance of the fibrous structure in the weld interface.[10] Additionally it has been shown through several experiments in a wide variety of friction welding conditions, that the deformation caused by the heat input during the upsetting stage and upsetting loss can be used to evaluate the joint performance in terms of tensile strength. Friction time, rotational speed and friction pressure must have high values to achieve sound joints. [11]

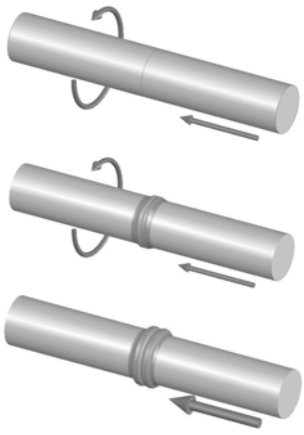

Figure 1: Schematic of the FW process.

[*] *G. Pinheiro, C.A.W. Olea, Dr. J.F. dos Santos and Prof. Dr. K.U. Kainer*
GKSS-Forschungszentrum Geesthacht GmbH
Institute for Materials Research- D-21502 Geesthacht, Germany
E-mail: gustavo.pinheiro@gkss.de
[**]The Authors gratefully acknowledge Dr. N. Hort for the fruitful discussions as well as Mr. V. Kree for the metallographic support during the course of this work. The financial support of the Brazilian Council for the Development of the Research (CAPES) is gratefully acknowledged.

Friction weldability of Mg based alloys has been worldwide discussed. Within this context the aim of this study was to investigate rotational friction welding of an Aluminum-Rare Earth based high creep resistance Mg alloy AE 42HP from the viewpoint of thermo cycle-microstructure-performance relationships to evaluate the potential use of FW in joining modern Mg-alloys.

Results and Discussion

Temperature measurements: Temperatures measured during FW in four different welding conditions, see Table 2, indicate at low welding pressures an increase of the total energy input with the rotational speed, since the resulting welding time was clearly longer. Holes with 1.2mm were drilled perpendicular to the main axis into the non-rotary studs to insert thermocouples at 5 and 10mm from the welding interface. An overview of the welding conditions and a summary of the peak temperatures for each welding condition 5mm away from the welding interface are presented in Figure 2. Longer welding times and consequently higher average maximum temperatures (out of 5 samples) reached by the welds performed within group Mg - 02 suggests a higher total energy input on those samples. In samples welded at higher friction pressures the maximum temperature and therefore the total energy input slightly decreases with rotational speed. Based on the results presented above, it can be concluded that the temperature varies randomly with rotational speed within the analyzed range of parameters.

Table 2: Summary of the weld parameter used within this work.

Sample	Welding Pressure (MPa)	Rotational Speed (rpm)	Forging Pressure (MPa)
Mg - 01	35	3000	55
Mg - 02	35	6000	55
Mg - 03	55	3000	75
Mg - 04	55	6000	75

When analysing the effect of the welding pressure on the total energy input, in both weld groups (at low and high rotational speeds) the temperature and consequently the total energy input decreased with the welding pressure. This tendency was observed since in the second group the preset burn-off is achieved faster owing to the higher welding pressure. Therefore the welding time is shorter and less heat is generated during the process. Generally Figure 2 shows that the longer the welding time is, the higher the temperature tends to be.

In both cases the range, in which the temperature varied, was always lower than 5%. Furthermore maximum temperature values recorded by the thermocouples closer to the bonding line hit values higher than those recorded by the thermocamera. On the one hand temperatures reached on the flash, where the camera is measuring, are noticeably lower than those in the middle of stud. As soon as the plasticized material is pressed out into the flash, convective thermal losses take place, which drops the temperature of the material in the flash down causing a lower indication on the camera. On the other hand the thermocamera system assumes the material has an emissivity equal to 1. As the emissivity of the material is obviously smaller and in large scale dependent on surrounding conditions, the temperature indicated by the camera is again lower than the real.

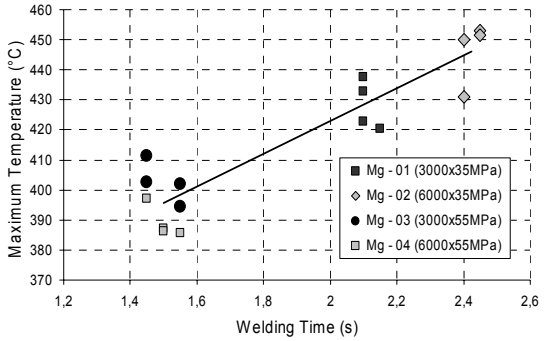

Figure 2: Variation of maximum temperature as a function of welding time.

Hardness: Microhardness scans carried out transversally to the weld interface showed higher hardness values on the bonding line region than those measured for the base material, as shown in Figure 3. This effect is possibly caused by the decrease of the grain size within this area as a consequence of the mechanical work imposed by the relative movement of the faying surfaces. The produced heat combined with this work-hardening effect produces a very fine dynamically recrystallized microstructure around the welding area. Such tendency of increased hardness in the weld area has been reported on the literature [11,14] and is associated in case of cast alloys with the formation of brittle second phase intermetallic particles.

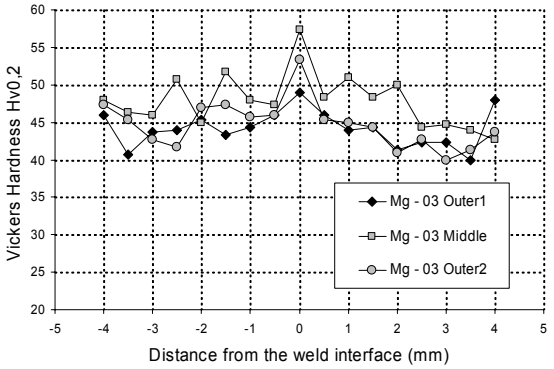

Figure 3: Micro-hardness profile along the welded joints.

From Table 3 a strong correlation between welding parameters and hardness values in an area 1mm around the weld interface can be observed. Generally longer welding times produce higher temperatures, which lead the joints to be subjected to a slower cooling rate and consequently to have on an average lower hardness values. Contrarily, welds performed with higher welding pressures showed the highest hardness level.

Table 3: Summary of the average hardness in relation to welding time and peak temperature.

Sample	Welding Time (s)	Maximum Temperature (°C)	Average Hardness (Hv0,2)
Base Material	---	---	40
Mg - 01	2,1	428	43,3
Mg - 02	2,4	446	41,6
Mg - 03	1,5	402	45,5
Mg - 04	1,5	389	47,0

Tensile tests: Tensile tests were also carried out to confirm the suitability of friction welding for performing sound welds in the selected base material. Figure 4 shows joints made under different welding conditions (see Table 2) having similar mechanical properties to those of the base material. No sample failed either at the bonding line or in the heat affected zone. Some observed loss of ductility can be attributed to an overmatch condition achieved in the weld region, which reduces the free length in which the sample is deformed. Tensile strength and elongation were found to be equivalent while the yield strength was in all the cases noticeably superior to that of the base material. Specimen Mg-04, where the lowest temperatures were measured, presented the highest tensile strength levels.

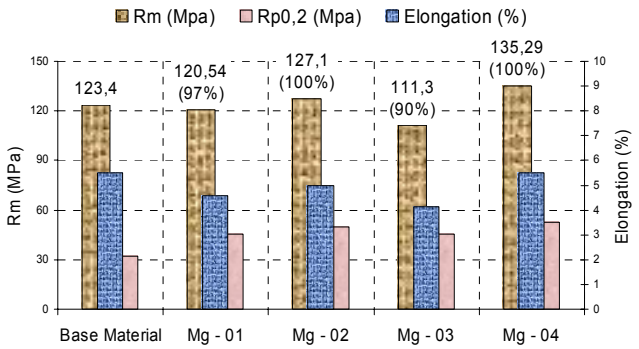

Figure 4: Tensile test results. Figures in brackets indicate the weld efficiency in reference to base material performance.

Although rotational speed is considered to have a minor influence on the formation of the weld interface [14], within this series, tensile strength increases clearly with rotational speed and has an undefined relation to axial pressure. Welds performed with slower rotational speeds presented efficiencies between 90 and 98% of the base metal, while samples 02 and 04 presented a 100% joint efficiency. On the other hand Figure 4 presents a randomly variation of the tensile strength with welding pressure. Additionally and contrarily to the results reported on the literature [14], fully satisfactory bonded joints from the perspective of tensile strength were obtained with short welding times (<3s).

Microstructure

Base Material: The microstructure aspects of the AE42 base material was initially investigated in order to understand the structural variations produced by the welding process. As recently reported [1,3,4], the as cast parent material presented a pronounced dendritic structure in the matrix in conjunction with dispersed lamellae and particulate second phase particles of $Al_{11}RE_3$, located preferentially along the grain boundaries. An overview of such structure is shown in the optical micrograph Figure 5(a). Details of the lamellae and particulate second phase particles obtained using scanning electron microscope (SEM) is presented in Figure 5(b). It can be observed that lamellae structure dominates the interdendritic microstructure. It has been reported that the presence of $Al_{11}RE_3$ hinder the formation of β phase $Mg_{17}Al_{12}$, improving significantly the creep resistance of the AE42 alloy.[2] Furthermore, it has been reported that rare earths in AE42 Mg alloys have also the potential to increase creep resistance by forming fine Mg_9RE second phase particles along the grain boundaries[4]. Additionally, the theory that AE42 creep resistance is due to the rare earth dissolved in Mg has not been experimentally supported since no evidence of rare earth solid solution has been found.[1] The material in as casting condition present equiaxed grains with a very coarse structure.

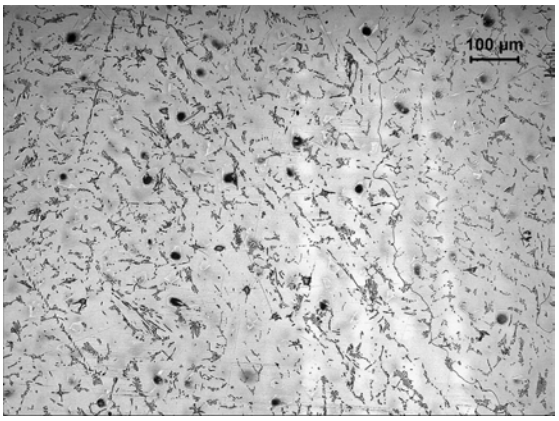

(a)

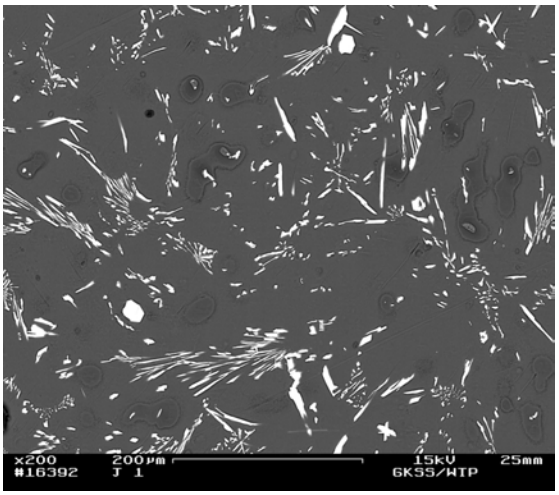

(b)

Figure 5: Microstructure of the die cast AE42 alloy base material. (a) Optical micrograph after etching in a solution of 20 ml distilled water, 100ml ethanol , 6-7ml glacial acetic acid and 12-15g Picric Acid. (b) Backscattered electron images of the lamellae structure.

Weld Zones: Macrostructural investigations of the welds indicate that sound welds with no porosity and without lack of bonding can be produced using friction welding (see Figure 6). A visibly clear bonding line was not identified for all four welded conditions suggesting an intimate contact between the workpieces imposed mostly by the forging pressure. In most cases a clear bonding line can be observed in the outer regions of the weld but not at the center, where a higher amount of plasticized material is usually concentrated. Such effect can be explained by the flow of plasticized material towards the cooler zones at an intermediate stage of the process (an intrinsic characteristic of the welding process). As the temperature of the material and consequently the width of the plasticized zone increase, the resistance to the axial force reduces and the excess of material is pressed out of the friction area although in lower amounts leading to a defined bonding line with less plasticized material in those regions.

The final microstructure of the friction welded joint has been carefully investigated and three main weld zones can be pointed out. Figure 6(a) shows a cross section macrograph of the joined AE42 where the different weld zones can be identified according to the local thermal history and degree of deformation. The weld zones are indicated in Figure 6(b) and identified as: HAZ – heat affected zone, where the microstructure and respective mechanical properties suffer only the influence of the heat generated during the welding process; TMAZ – thermo-mechanical affected zone, where the peak temperature is higher and grains experience a substantial deformation, generally resulting in recovery of the highly strained grains and the RZ – recrystallized zone, which is distinctly characterized by formation of a fine grain microstructure with equiaxed morphology as a product of the dynamical recrystallization phenomenon. The refined microstructure of the recrystallized zone resulting from the welding process is shown in Figure 6(c).

Bethlehem [15] reported that the region between 0.3 and 0.7 of the stud radius undergo severe deformation and heating during the first stage of the welding. The further increase of the temperature in this ring area causes the squeezing of highly plasticized material to cooler region of the friction area. The local low temperature of the cooler region produce immediate cooling of the plasticized material and intense friction is again generated in this particular region extending the ring area firstly towards the rotational center. The temperature in the center area is comparatively lower, because of the low relative speed and therefore because of the low heat generated between the rubbing faces at this point. The macrographs of all welding conditions showed that the width of the recrystallized layer in the center of the stud was always greater than that of the recrystallized layer at the border. In order to evaluate the influence of the welding parameters on the geometry of the recrystallized zone, the thickness of the recrystallized layer has been measured through the whole welding interface. According to the measurements carried out using light microscope, it was also evident that the rotational speed plays an important role on the amount of heat generation. Welds carried out using low rotational speeds shown a noticeably higher amount of recrystallized material if compared to welds carried out with high rotational speeds. On the other hand it was not possible to observe a significant variation in the welds made using low and high welding pressure.

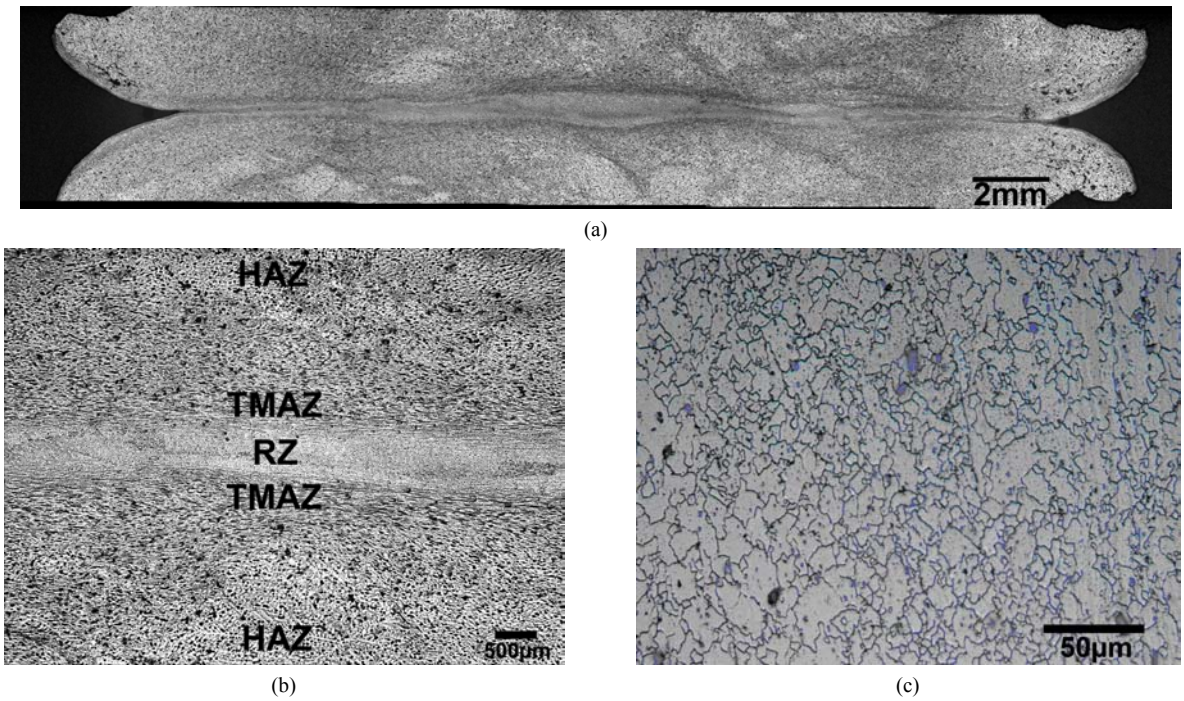

Figure 6: Interface of a friction welded similar AE42 joint. (a) Macrograph of the cross section showing an overview of the join; (b) Micrograph detailing the weld zones with respective microstructural gradient and; (c) Equiaxed grains observed in RZ.

Grain Size: Measurements of the average grain size were performed in the base material and recrystallized zone. The grain size of the base material in as cast condition has shown a large coarse structure with average size of about 2130µm. The average grain size in the recrystallized zone has been found to be smaller in the center area than next to the border area, as shown schematically in Figure 7. According to the diagram, the average grain size in the weld center has shown to be about 8µm for low welding pressure, while for high weld pressures it has shown to be about 5µm. Similar decrease in the average grain size with the increase in welding pressure was found in the border area of the recrystallized zone, with grains of about 11µm and 8-9µm for the low and high welding pressures, respectively. This is probably due to the relative speed and therefore the perceptibly higher heat generation in the outer regions of the friction interface. Although welding time and maximum temperature have shown different values on the samples welded at low pressures, grain size was very similar in both cases. The major difference in grain size measurement was observed between specimens welded at high pressures. According to the results, rotational speed seems not to play a significant role on the final grain size/microstructure of the recrystallized zone.

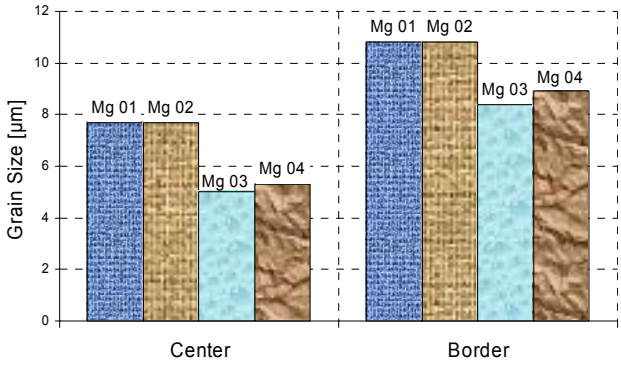

Figure 7 – Diagram showing in the center and in the outer areas the grain size variation in the recrystallized zone according to the welding condition.

On the other hand, it was observed that the pressure affects directly the microstructural evolution of the AE42 alloy. In both cases, the higher the welding pressure, the smaller the average grain size. Comparing the welds produced under different conditions, it was observed that generally samples with coarser grain size reached the highest temperatures, i.e. the increase in welding temperature correspond to a coarser grain size. The grain coarsening observed in the highest temperatures can be easily elucidated in terms of the high diffusion of atoms across the grain boundaries.

Nevertheless, in the recrystallized zone, slight grain growth can be observed in a region adjacent to the TMAZ. The recrystallized zone extends in the center an average thickness of 1.15 mm (depending on welding parameters), presenting thicker layer in welding condition Mg-01, and thinner layer in condition Mg-02. The border region is characterized by an average thickness of 0.43 mm, again presenting thicker layer in welding condition Mg-01, and thinner layer in condition Mg-03. The welding parameters and the thickness of the recrystallized zone layer seem not to be in a proportional correlation. Although, in general, it was suggested that low rotational speed tends to increase the thickness of the recrystallized zone layer.

Interdendritic particles and weld interface: As shown in this work and also in accordance with previous investigations[1], grain boundaries of AE42 base material microstructure contain extensive precipitation of second phase particles with lamellar morphology dominating the interdendritic microstructure in the unaffected base material (see Figure 8). After the friction welding process, SEM analyses indicate a complete disintegration of the lamellae structure along the recrystallized zone, being extended partially to the TMAZ. Such phenomenon can be expected since the temperature attained during the process is still low to promote considerable diffusion and/or dissolution of the brittle (Al-RE, Mg-RE) intermetallic lamellae compounds. Thus, the massive degree of deformation applied to the weld interface caused by the relative movement between both studs associated with welding pressure during the joining process produce mechanical fragmentation of the $Al_{11}RE_3$, as can be observed in the backscattered electron image of Figure 8.

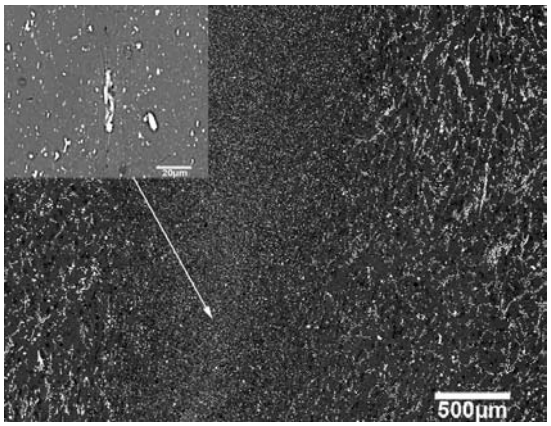

Figure 8 – SEM micrograph of the recrystallized zone showing the mechanical fragmentation of the lamellae particles.

A detail of the second phase particles fragmented in the middle of the recrystallized zone is shown in Figure 8. The SEM image also reveals in detail that an amount of broken particles with different sizes were randomly distributed along the magnesium matrix. In some welding conditions it was possible to observe clusters of particles in particular places along the bonding line. This particles concentration over the bonding line appears probably due to the superior hardness of the intermetallic compounds when compared to the Mg matrix. It was verified that mechanical work and peak temperatures were not enough to mechanically

dissolve such particles and also that the hydro-extraction effect was not effective to expulse them from the faying surfaces. As such phases, due to the axial shortening, are pushed into the weld interface and grouped over it, a structure similar to a lack of bonding is formed exactly over the bonding line. In welds produced with higher rotational speeds and pressures such clusters are fragmented and could not be observed even under higher magnifications.

Conclusions: This investigation has demonstrated that sound welds with no porosity and without lack of bonding can be produced using friction welding. Weld interface in all cases shows the pattern of a typical friction welded joint. The microstructure at the bonding line is characterized by a thin layer of dynamically recrystallized grains without any special particles or phases precipitated at grain boundaries. After the friction welding process, SEM analyses indicate a complete disintegration of the lamellae structure along the recrystallized zone, being extended partially to the TMAZ. Average grain size was always smaller in the center than on the periphery of the weld. Also rotational speed seems not to have a significant influence on the grain size of the welding zone. On the other hand the higher the welding pressure, the smaller the average grain size. Samples with larger grains reached the highest temperatures.

It was observed that welding pressure plays an important role in the course of the process and consequently in the formation and properties of the joint. On the other hand the rotational speed seemed not to influence significantly the welding process. Welding temperature varies randomly with rotational speed within the analyzed range of parameters. The effect of the welding pressure on the total energy input showed that the temperature and consequently the total energy input decreased with the welding pressure

Hardness tests confirm an overmatching condition at the welding interface. Additionally, within the range of parameters investigated fully satisfactory bonded joints from the perspective of tensile strength were obtained. No sample failed at the bonding line and no joint faced the problem of ductility loss (at 100% joint efficiency).

Experimental

An AE42-HP (high-purity) alloy has been selected for the present study. The material was delivered as cast ingots and spark-eroded. Table 4 lists both its mechanical properties according to tests carried out at GKSS and to the literature.[7]

Table 4: Mechanical Properties of base material.

Material	Rm (MPa)	Elongation (%)	Hardness (Hv0,2)
AE42HP	125 (114 - 143)	6 (4 - 7)	40 (36 - 44)
AE42 [7]	234	11	60

Conventional cylindrical geometry was chosen for this work with 20mm diameter and 100mm length studs. The rotating stud was tightened to the weld head while the other was remained stationary. This geometry was suitable to fit in the friction welding machine and is commonly used to perform conventional friction welding trials. Additionally, 1.2mm holes were drilled perpendicular to the main axis into the non-rotary studs to insert thermocouples at 5 and 10mm from the welding interface.

A HSM 3000 machine has been used to perform the welds. This is a portable hydraulic powered friction welding system, designed and built by Circle Technical Services Ltd. Before the beginning of the welding operation itself some procedures were followed in order to ensure the reproducibility of the welding programme and to avoid as much as possible external influences. The studs were cleaned with acetone to eliminate all possible contaminations forms that could influence the weld results. The oil temperature of the machine was kept at 20+-2°C prior to the beginning of the weld in order to avoid significant changes in the power delivered by the welding machine. Four individual friction welding conditions were investigated according to Figure 2. The used upset was 5.0mm with the forging pressure always 20MPa higher than the welding pressure. Each set of parameters, i.e. each weld of the weldability matrix was performed five times. Four specimens of each weld were designated to tensile tests and the remaining one to metallographic analysis including grain size measurements. Thermal cycles were recorded in all cases using both thermocouples and an infrared camera.

Welded specimens were cut (longitudinally, in the center of the studs) and etched. Finally hardness and tensile tests has been carried out on specimens with the bonding line positioned in the middle of gauge length.

[1] B.R. Powell, V. Rezhets, M.P. Balogh and R.A. Waldo, *JOM August* **2002**, *34-38*.

[2] I.P. Moreno, T.K. Nandy, J.W. Jones, J.E. Allison and T.M. Pollock, *Scripta Materialia* **2003**, *48, 1029-1034.*

[3] H. Dieringa, A. Bowles, N. Hort and K.U. Kainer, *Materials Science Forum* **2005**, *482, 271-274*.

[4] Y. Huang, N. Hort, H. Dieringa and K.U. Kainer, *Advanced Engineering Materials* **2004**, *6(11), 883-888*.

[5] H. Dieringa, N. Hort and K.U. Kainer, *Kompozyty/ Composites* **2003**, *3, 275*.

[6] P. Bakke, A.L. Bowles and H. Westengen, *7th International Conference on Magnesium Alloys and their Applications* **2006**, *53-66.*

[7] ASM Handbook, Magnesium and Magnesium alloys, **1999**, *17*.

[8] J.G. Kaufman, *Properties of Aluminum Alloys,* **1999**, *41 and 131*.

[9] A. Bowles, N. Hort, A. Meyer, J.F. dos Santos and K.-U. Kainer, *6th International Conference on Magnesium and their Applications, September* **2003**, *917-923.*

[10] K. Kato and H. Tokisue, *Welding International,* **1994**, *08, 452-457*.

[11] K. Ogawa, H. Yamaguchi, H. Ochi, T. Sawai, Y. Suga and Y. Oki, *Welding International,* **2003**, *17, 879-885*.

[12] U. Draugelates, A. Schram, B. Bouaifi and Chr. Kettler, *Institute of Welding and Machining (ISAF),* **1998**, *TU-Clausthal, Germany.*

[13] K. Kato and H. Tokisue, *Welding International,* **2004**, *18, 861-867.*

[14] U. Draugelates and A. Schram, *Institut für Schweißtechnik und Trennende Fertigungsverfahren,* **2000**, *TU-Clausthal, Germany.*

[15] Bethlehem, W., *Schweißen und Schneiden, **1984**, 36(10), 479-483.*